

## Design Techniques of Microwave Filters:

### A Literature Review

Ashna shaiba<sup>1</sup>, Dr. Agya Mishra<sup>2</sup>

<sup>1</sup>Department of Electronics & Telecommunication Engineering, Jabalpur Engineering College, Jabalpur Madhya Pradesh, Pin- 482011 India

<sup>2</sup>Department of Electronics & Telecommunication Engineering, Jabalpur Engineering College, Jabalpur Madhya Pradesh, Pin- 482011 India

#### Abstract

Microwave filters are widely used in telecommunication equipments. Filters are used to suppress the noises coming from the environment, prevent spurious signals from interfering with other systems and allow desired signals to pass through within a specific frequency band. Filters in this work, the filters working particularly in microwave frequency range i.e. several MHz to GHz range according to their designing and applications i.e. chebyshev filters, cavity filters etc is critically reviewed. For designing a filter satisfying the design specification an to obtain low complexity used the 2-D IIR filter i.e. RF-to-bits antenna array digital beam filters which rectifies the non-linearity in the phase response. This paper gives critical review of designing techniques of microwave filters..

**Keywords:** Microwave filters, 2-D IIR filters, cascaded filters, cross-coupling, polarimetric synthetic aperture radar(PolSAR), speckle suppression, target detection.

#### 1. Introduction

A filter is an electronic device used to select a particular pass band range. Signals with in that range are allowed to pass while the signals outside that range are disallowed. In state-of-the-art RF receivers, high performance filters are required to remove undesired signals at different stages of the receiving process, such as noise from incoming signals the antenna receives, undesired signals at image frequency, and harmonics after mixing operation. The most common filter responses are the Butterworth, chebyshev, Elliptic, Bessel types etc. The filters are used for different applications in their range. Also, it is very important to reduce the losses like insertion loss and return loss in various communications. For that we have used the chebyshev filters [2] and 9<sup>th</sup> order chebyshev filter [5] since it gives the better response. With the fast development of wideband wireless communication, Bandpass filter (BPF) with characteristics of high performance low-cost, low insertion loss(IL) and compact

BPF are highly desirable here we have used fifth order chebyshev BPF which outputs the filter dimensions for the required centre frequency(10 GHz to 12 GHz) and bandwidth(6 to 12%).

Cavity filters are the basic circuitary behind a duplexer and are sharply tuned resonant circuit that allow only certain frequencies to pass. Generally filter of this kind are known as notch filters widely used with broadly tunable cavity filter at UHF up to 700 MHz range and become more practical in terms of size and significantly higher quality factor than lumped element resonators and filters. The fields of 2-D digital signal processing and digital image processing found new applications to expand in areas such as communications, consumer electronics, robotics, geophysics etc. the paper presented below is related to the synthesis of the 2-D IIR response filters using model order reduction. After that 2-D IIR digital beam filter is employed as a pre-processing stage to existing phased/timed arrays, thereby mathematically modifying the array transfer function. The reconfigurable phase-linearizer for 2-D IIR RF-to-Bits antenna-array digital beam filters approximately rectifies the non-linearity in the phase response using an FFT-based phase compensation method with frequency range up to 315 MHz range. At last the extended polarimetric whitening filter (EPWF) for target detection in polarimetric synthetic aperture radar (PolSAR) images. Specially for single-look and multilook PolSAR data, the Guassian mixture model (GMM) and Wishart mixture model (WMM) are applied.

#### 2. Microwave Filters and Performance Algorithm

Various filters working in microwave frequency range are discussed as per the designing purposes and applications.

The various filters used are-. 5th order chebyshev filter for dimension scaling and tuning of microwave filters using formulation of feature-based optimization algorithms and construction of inverse surrogate model [1], . Chebyshev filters of 9th order for design of low pass filter(LPF), high pass filter (HPF) and BPF using UVB and X-band and comparison with MATLAB coding using EM circuit simulator [5], . Chebyshev BPF using cavity combline filter-low pass prototype conversion into combline and presented using HFSS [6], 2-D IIR filters for wireless communication applications-combined time delay FIR and IIR filter for wireless communication examples- RF-to-BITS antenna array digital beam filters up to 315 MHz, spatial image rejection filter for J-band radar applications, the extended polarimetric whitening filter for speckle suppression in clutter region, target detection and thresholding [9] [11] [12] [13] etc.

### 2.1 Inverse surrogate modeling for dimension scaling

Let  $x_B^{(k)}$ ,  $k=1, \dots, N_B$ , be the reference designs obtained for the center frequencies and bandwidths  $f_0^{(k)}$  and  $B^{(k)}$  respectively. Here, these designs are obtained at a low cost using the feature based optimization (FBO) algorithm. We define the inverse models  $x_s^{(j)}(f,B)$ ,  $j = 1, \dots, n$  (n being the number of design parameters) by solving the regression problems in [1] as:

$$\min_1 \sum_{k=1}^{N_B} [x_s^{(j)}(f_0^{(k)}, B^{(k)}) - x_{B,j}^{(j)}]^2 \quad (1)$$

for  $j = 1, \dots, n$ , with respect to the model parameters (not shown explicitly for the sake of keeping the notation simple). The overall inverse model is then defined as:

$$x_s(f_0, B) = [x_s^{(1)}(f_0, B) \dots x_s^{(n)}(f_0, B)]^T \quad (2)$$

The model above provides the initial estimation of the dimensions of the filter scaled to the center frequency  $f_0$  and the bandwidth  $B$  of interest. Here, we use nine reference designs arranged on a  $3 \times 3$  uniform grid with respect to the scaling range  $[f_{0min}, f_{0max}]$  and  $[B_{min}, B_{max}]$ . The inverse models are second order polynomials so that the model parameters can be found analytically.

### 2.2 Dimension scaling algorithm

The proposed procedure has two stages: (i) obtaining the reference designs and constructing the inverse model, (ii) filter scaling. Stage (i) is executed only once for a given filter structure and scaling range. Then, the results can be reused at essentially no cost. The second stage has two steps:

- Obtain an initial geometry of the scaled filter by evaluating the inverse model  $x_s(f_0, B)$ ;
- Tune the filter using the algorithm with the feature model surrogate.

### 2.3 Low pass prototype conversion in to combline and presented and simulated using HFSS

It is presented how to derive the L,C resonator starting from a low-pass prototype coupling matrix, which consists of a unity capacitance and frequency-invariant susceptance (B). Once the L and C values are obtained, the next step is to find the combline equivalent circuit, as summarized in Fig. 1, with capacitance (Cc) and short-stub admittance (Yr). Derivation of the combline equivalent of the (L,C) resonator is presented, resulting in a shunt capacitance Cc and short-stub admittance Yr. The well-known susceptance slope parameter method is applied to convert the lumped element resonator values into the combline parameter values. Equating the express Cc and Yr in terms of each other in [6]. That is

$$Y_1(\omega)|_{\omega=\omega_0} = Y_2(\omega)|_{\omega=\omega_0} = 0$$

$$\Rightarrow j\omega_0 C + \frac{1}{j\omega_0 L} = j\omega_0 C_c + \frac{Y_r}{j \tan(\theta)} = 0. \quad (3)$$

Equation (2) expresses the equivalence of the slope of the admittances at the resonant frequency as

$$\frac{dY_1(\omega)}{d\omega} \Big|_{\omega=\omega_0} = \frac{dY_2(\omega)}{d\omega} \Big|_{\omega=\omega_0}$$

$$\Rightarrow \left( C + \frac{1}{\omega_0^2 L} \right) = C_c + \frac{Y_r \ell}{\nu \sin^2(\omega_0 \frac{\ell}{\nu})} \quad (4)$$

where the short-stub impedance is  $Z_{ss}(\omega) = jZ_r \tan(\beta l)$  with  $\theta = \beta l = \omega(l/\nu)$ .  $l$  and  $\nu$  represent the length of the stub and the propagation speed, respectively. The two unknowns Cc and Yr are derived using the two equations (3) and (4), as:

$$Y_r = \frac{2C}{\left[ \frac{1}{\omega_0 \tan(\theta)} + \frac{\ell}{\nu \sin^2(\theta)} \right]} \quad (5)$$

$$C_c = \frac{2C}{1 + \frac{\omega \ell}{\nu \sin(2\theta)}} \quad (6)$$

The next step is impedance scaling, which is done by means of the scaling factor for every resonator taking into account the nominal  $Z_0 = 76 \Omega$  value as the reference coaxial stub impedance. Scaling factor is given by

$$n_r = \sqrt{\frac{Y_0}{Y_r}}, \quad r = 1, \dots, N \quad (7)$$

where N denotes the number of resonators, and  $Y_0 = 1/Z_0$ . Following the scaling, the network parameters are

modified accordingly together with the inverters representing the couplings. Inverter models are combined with the resonators to finalize the circuit configuration. Positive and negative couplings are modeled as pi-section stubs and capacitance values, respectively. Once the equivalent models replaced the inverters, the combined network parameters as well as input and output couplings are calculated using the derivations, as

$$Y_{input(i)} = Y_{output(o)} = 1 - \frac{1}{n_1 \cos(\theta)}$$

$$Y_{s1} = Y_{NL} = \frac{1}{n_1 \cos(\theta)}$$

$$Y_1 = Y_N = (Y_0 - Y_{12}) + \frac{1}{n_1^2} - \frac{1}{n_1 \cos(\theta)} \tag{8}$$

A network schematic with input, output, and interresonator couplings ( $Y_{r,r+1}$ ) together with the stub admittances ( $Y_r$ ) is shown in Fig. 1. In the figure, we have

$$Y_r = Y_0 - Y_{r-1,r} - Y_{r,r+1} - Y_{r,t} \text{ for } r > 2, r < N \tag{9}$$

where  $Y_{r,t}$  refers to the admittance introduced through any cross-coupling between resonator  $r$  &  $t$ .

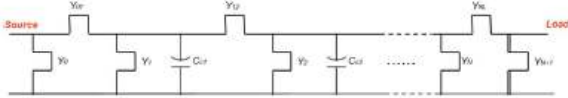


Fig. 1. Coupled combline network [6]

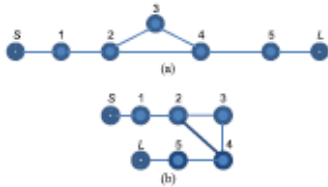


Fig. 2. Each node represents a resonator. (a) Inline topology. (b) Folded topology in [6]

Individual filters are synthesized, such that each one of them has a transmission zero on either side of the passband. The result of the responses of the two cascaded asymmetrical filters is a sharper and narrower bandpass, which can only be obtained with a very high-order number ( $N$ ) filter, otherwise. To obtain a sharper skirt on both sides of the passband, asymmetric transmission zeros are introduced. Cross-coupling results in transmission zeros. The design method is applied to prevent the deteriorating effect due to mismatch between the filters. The idea is to share a central resonator by eliminating the need for an isolator. The last resonator of the first filter and the first resonator of the second filter are combined and replaced by an equivalent resonator.

## 2.4 Semi-definite programming approach to obtain a low complexity IIR filter using model order reduction

The problem of IIR filter design is to determine a rational and stable function  $H(z_1, z_2)$  with a wedge support output mask that meets a given design specification. In other words, we wish to determine a stable computational procedure that is recursively computable and meets a design specification. However, a given rational system function  $H(z_1, z_2)$  can lead to many different computational procedures [7]. To make the relationship unique, we will adopt a convention in expressing  $H(z_1, z_2)$ .

Specifically, we will assume that  $a(0,0)$  is always 1, so  $H(z_1, z_2)$  will then be in the form

$$H(z_1, z_2) = \frac{\sum_{(k_1, k_2) \in R_b} b(k_1, k_2) z_1^{-k_1} z_2^{-k_2}}{1 + \sum_{(k_1, k_2) \in R_a, -(0,0)} a(k_1, k_2) z_1^{-k_1} z_2^{-k_2}} \tag{10}$$

where  $R_a \rightarrow (0,0)$  represents the support region of  $a(k_1, k_2)$  without the origin  $(0,0)$ , and  $R_b$  represents the support region of  $b(k_1, k_2)$ .

The unique computational procedure corresponding to (10) is then given by

$$y(n_1, n_2) \leftarrow - \sum_{(k_1, k_2) \in R_a, -(0,0)} a(k_1, k_2) y(n_1 - k_1, n_2 - k_2) + \sum_{(k_1, k_2) \in R_b} b(k_1, k_2) x(n_1 - k_1, n_2 - k_2) \tag{11}$$

where the sequences  $a(k_1, k_2)$  and  $b(k_1, k_2)$  are the filter coefficients, and  $x(.,.)$  is the input signal.

The first step in the IIR filter design is usually an initial determination of  $R_a$  and  $R_b$ , the support regions of  $a(k_1, k_2)$  and  $b(k_1, k_2)$ . If we determine the filter coefficients by attempting to approximate some desired impulse response in the spatial domain, we will want to choose  $R_a$  and  $R_b$  such that  $h_d(n_1, n_2)$  will have at least approximately the same support region as  $h_d(n_1, n_2)$ .

Another consideration is related to the filter specification parameters. In the low pass filter design, for example, small (filter templates) and transition region will generally require a larger number of filter coefficients. It is often difficult to determine the number of filter coefficients required to meet a given filter specification for a particular design algorithm, and an iterative procedure may become necessary [7]. In the 1-D case, there are two standard approaches to designing IIR filters. One is to design the filter from an analog system function, and the other is to

design directly in the discrete domain. The first approach is typically much simpler and more useful than the second: using an elliptic analog filter's function and a bilinear transformation. Unfortunately, this approach is not useful in the 2-D case. In the 1-D case, this approach exploits the availability of many simple methods to design 1-D analog filters. Such simple methods do not exist for designing a 2-D analog filters. The second approach for designing IIR filter directly in the discrete domain can be classified into two categories. The first is the spatial domain design technique, where filters are designed by using an error criterion in the spatial domain. The second is the frequency domain design technique, where filters are designed by using an error criterion in the frequency domain. Therefore, the weighted Chebyshev error criterion, also known as the min-max error criterion, is a natural choice for designing IIR filters. An error criterion of this type, however, leads to a highly nonlinear problem [7,8].

2.5 2-D IIR pre-filtering stage for reduced side-lobes

We exploit the complex pole-manifolds in the 2-D IIR transfer function to obtain additional spatial selectivity (i.e. reduced SLL) by employing the 2-D IIR beam filter as a pre-filtering stage to conventional phased arrays. The complete system transfer function is therefore given by [9] is

$$H(z_x, z_{ct}) = H_{FIR}(z_x, z_{ct})H_{IIR}(z_x, z_{ct}). \tag{12}$$

The array factor corresponding to  $H(z_x, z_{ct})$ , where the reduced SLL (without compromising the main lobe directivity for the same number of antennas) is observed.

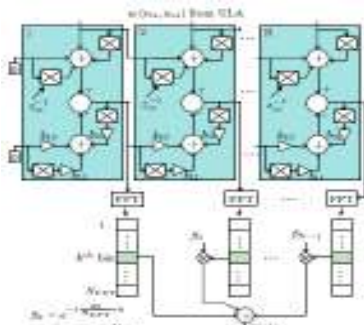


Fig. 3 Detailed SFG of  $H(z_x, z_{ct})$  in [9]

In a typical radar/communication application, the projected improvement in the SLL will be reflected as an additional gain in the signal to interference ratio (SIR). Fig. 3 shows the complete SFG of the system, where the 2-D IIR beam pre-filter is realized as a systolic array architecture

comprising  $N$  identical processing modules. The first processing module is provided with zero valued spatial inputs (initial conditions) as required by the p-BIBO stability of  $H_{IIR}(z_x, z_{ct})$ .

2.6 FFT-based phase compensation method

We propose a phase compensator that operates by applying a phase-rotation to every bin of an  $N$ -point discrete Fourier transform (DFT) of the output sequence, obtained from the preceding 2-D IIR beam filter. We design the phase compensator such that its phase response is equal to the deviation from the desired linear phase response of the preceding 2-D beam filter along the beam axis direction. By ensuring a unit magnitude response, the phase compensation algorithm will not affect the magnitude of the filters output signal spectrum. The architecture of the proposed phase compensator is shown in Fig. 4. Note that, the 1-D beamformed output signal of the beamformer given by [11] is,

$$\omega_x = -\omega_k \tan \theta = -\omega_k \sin \psi \tag{13}$$

The 1-D transfer function of 1st-order 2-D beam filter computed along the passband axis direction for  $k$ th frequency bin can be found as,

$$H_1(e^{j\omega_k \tan \theta}, e^{-j\omega_k}) = \frac{(1 + e^{j\omega_k \tan \theta})(1 + e^{-j\omega_k})}{1 + \sum_{k=0}^1 \sum_{l=0}^1 b_{kl} e^{j k \omega_k \tan \theta} e^{-j \omega_k l}} \tag{14}$$

It follows that the phase response of for the cases of 2nd order filter order becomes,

$$H_2(e^{j\omega_k \tan \theta}, e^{-j\omega_k}) = \frac{(1 + e^{j\omega_k \tan \theta})^2 (1 + e^{-j\omega_k})^2}{1 + \sum_{k=0}^2 \sum_{l=0}^2 b_{kl} e^{j k \omega_k \tan \theta} e^{-j \omega_k l}} \tag{15}$$

Thus, the linearized phase of  $k$ th frequency bin of  $N$  coefficients is denoted as,

$$\omega_k = -\frac{2\pi}{N} k \tag{16}$$

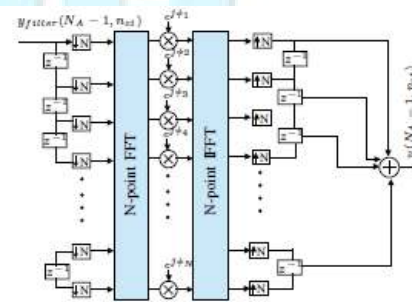


Fig. 4 The architecture of the real-time phase compensator.[11]

Then, the phase error for the frequency bin is given by,

$$\phi_k = \omega_k - \angle H(e^{j\omega_k \tan \theta}, e^{-j\omega_k}) \tag{17}$$

Following rotation, the output signal in the time domain is derived employing the inverse Fourier transform (IFFT). The proposed phase compensator VLSI architecture is shown in Fig. 3 where a multirate structure is used for packetization of the filtered output samples for N-point block processing in the phase compensator. In our rapid prototype, we use standard FFT and IFFT cores from Xilinx to achieve the DFT and inverse DFT operations in real-time. However, the implementation that results is time multiplexed. That is, it uses folding operations to achieve low complexity at the cost of latency in the filtered output.

### 2.7 Miniaturized-element frequency selective surface (MEFSS) for image suppression

The membrane-supported FSS structure was fabricated using microfabrication technology. First a 10micrometer thick layer of a low loss polymer membrane is deposited on a wafer. The MEFSS element are then patterned over the membrane and grown to the desired thickness using gold electroplating technique. At the last step, the membrane-supported structure is released from the carrier wafer and glued to a holder as shown in fig. 5. Transmission response of the fabricated structure is obtained experimentally using a free-space measurement setup composed of a network analyser(PNA-X) and OML MMW frequency extenders. Fig. 6 shows that the measured transmission response has 0.6 db insertion loss in the passband and more than 25db rejection around the lower side-band which is in good agreement with numerical simulations of both the structure and its circuit model.

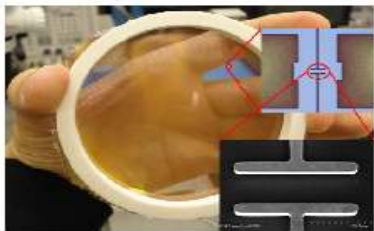


Fig. 5. Photos of fabricated membrane-supported MEFSS [12]

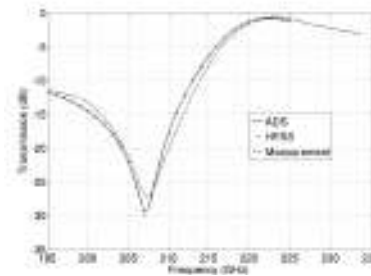


Fig. 6 Measured and simulated transmission response of membrane-supported MEFSS[12].

### 2.8 Finite mixture models for modeling PolSAR clutter

In the proposed detection scheme, we use the Gaussian mixture model (GMM) and Wishart mixture model (WMM) to fit, respectively, single-look and multilook PolSAR data. Suppose that the mixture model is composed of M components, each being associated with a covariance matrix  $C_m$  and a weight  $\pi_m$ ,  $m = 1, 2, \dots, M$ . The pdf of the GMM is the weighted sum of M complex Gaussian distributions in [13], i.e.,

$$p(\mathbf{k}; M, C_1, \dots, C_M, \pi_1, \dots, \pi_M) = \sum_{m=1}^M \pi_m \frac{\exp\{-\mathbf{k}^H C_m^{-1} \mathbf{k}\}}{\pi^D |C_m|} \tag{18}$$

Similarly, the pdf of the WMM is the weighted sum of M complex Wishart distributions, i.e.,

$$p(\mathbf{Z}; M, C_1, \dots, C_M, \pi_1, \dots, \pi_M) = \sum_{m=1}^M \pi_m \frac{L^{LD} |\mathbf{Z}|^{L-D} \exp\{-L \text{Tr}(C_m^{-1} \mathbf{Z})\}}{\Gamma_D(L) |C_m|^L} \tag{19}$$

For simplicity in this letter, the number of mixture components is set by the Bayesian information criterion (BIC) although such value can be determined by more elegant strategies such as the goodness-of-fit test. The covariance matrices and weights are estimated using the expectation-maximization algorithm. In previous studies, the Gaussian model and compound Gaussian model were commonly used when statistical models for PolSAR data were needed. They are collectively referred to as the scale mixture of Gaussian (SMoG) model, the infinite mixture components of which are continuously indexed by a scalar texture variable that is shared across all polarization channels. As a resulting limitation, the SMoG model may not be able to fully characterize highly nonhomogeneous regions where different polarization channels are modulated by independent texture variables. The GMM and WMM that we propose make no specific assumptions on

the texture. They can have an independent SMR for each polarization channel and generically fit all kinds of PolSAR data.

### 3. Comparison Of All Existing Algorithm

The below comparison table of design techniques of existing microwave filters gives the measuring parameters and certain values required in the designing of filter. In this, almost all the filters works on microwave frequency range. The chebyshev filter of fifth order used in this table is applied for dimation scaling and tuning of microwave filters. Likewise to maintain good impedance match for more than octave tuing range is provided by cavity filter and to get narrow band filter response combine filter is used. Also, the comparison of 2-D IIR filters available are compared as per different applications in wire and

wireless communications to provide minimum insertion loss and signal supression, target detection, thresholding etc.

### 4. Conclusions

In this work, microwave filters and their needs in various application is critically reviewed and these reference paper results that by using the chebyshev filter of fifth order for dimension scaling and tuning of microwave filter has inaccuracies due to high sensitivity of filter characteristics. Also, the state space realization are not possible for all 2-D IIR filter transfer function. Although the combined time delay FIR and IIR filters achieves electronically scanned beams, rectifies the non-linearity in the phase response but has the disadvantage of frequency warping and magnitude response is distorted at higher frequency.

**Table 1: COMPARISON OF DESIGN TECHNIQUES OF MICROWAVE FILTERS**

S. No.	Name of technique/ method used	Applied for What	Frequency Range For	Measuring Parameters & Values	Advantages	Disadvantages
1.	Fifth order Chebyshev band pass filter [1]	Dimension scaling and tuning of microwave filters ,outputs the filter dimensions for required centre frequency and bandwidth	10GHz-12GHz (Tuning Range)	Centre frequency $f_0=10\text{GHz}-12\text{GHz}$ & BW=6% to 12%	Low cost procedure, simple design problem, rapid design tuning of initially scaled filter	Due to high sensitivity of filter characteristics any inaccuracy leads to deviation from ideal characteristics
2.	Cavity filter [3] [4]	Piezo-electric tuning of capacitively loaded cavities, to maintain good impedance match more than octave tuning band, broadly tunable filter with very low loss at UHF	300MHz-700MHz	Mid band losses=0.5 to 0.9db Quality factor=340-550 Loss range=0.9db at 300MHz 0.7db at 700MHz (with lowest loss of 0.5-0.6db at mid-band)	Maintain good impedance match for more than octave tuning range, provide capacitive loading without introducing additional losses	
3.	9 <sup>th</sup> order Chebyshev filter(BPF, LPF ,HPF) [2] [5]	To design a microwave filter working on a general frequency range	For UWB-3.1to 10.6GHz For X-band-8-12GHz	For all filters- S <sub>21</sub> ~0db(Insertion loss) S <sub>11</sub> ~-10db(Return loss)	Peak error minimized and equiripple magnitude response in the passband monotonically decreasing magnitude response in stopband, sharp roll-off than butterworth filter	
4.	Combine Filter (with cross-coupling based on chebyshev BPF) [6]	To get a tunable Narrow-band filter response and flexible bandwidth	Stopband - below 1900 & above 2100MHz Passband - 1.96-2.04 GHz	BW & Centre frequency. 1 <sup>st</sup> filter- BW=20MHz Centre frequency=1.98GHz & 2 <sup>nd</sup> filter BW=20 MHz Centre frequency=2.03GHz	Saved the weight, reducing cost, to deteriorate the effect due to mismatch between the filters	

5.	2-D IIR Filter [7] [8]	To design a filter satisfying the design specification, obtain a low-complexity filter		The numerator and denominator matrices, filter order(n,m)=(13,13), reduced order(8,8)	Recursively computable, reduced memory requirements, balanced realization	State-space realization are not possible for all 2-D T.F.
6.	Combined Time-delay FIR and 2-D IIR Filter [9]	To improve the Spatial Selectivity of existing aperture array beamformers (2-10db improvement)		Closed form frequency response, aperture beamformer for N=32 antennas & beam direction =25degrees temporal frequency= $\pi/2$	Proposed beamformers to additional gain of >10db, for ultra-wide band Beamforming application, useful in wire comm. simulation	
7.	RF-TO-BITS Antenna array Digital beam Filter [11]	To achieve electronically scanned RF beams, rectifies the non-linearity in the phase response	Up to 315MHz	Phase responses, N=256 point Critical path delay T=3.17ns	Magnitude smaller multiplier complexity, linearises the responses at higher frequency imaging and wireless comm. app.	Frequency warping, magnitude response is distorted at higher frequency
8.	Spatial image Rejection filter [12]	For suppressing image response of J-band up-converter mixer, suppress lower sideband, provide minimum insertion loss	Passband – 221-223 GHz, Sig. suppression range-205-207 GHz band	Insertion loss in the passband=>25db rejection	To provide minimum insertion loss & signal suppression, harmonic response are eliminated	Ohmic loss
9.	The Extended Polarimetric whitening filter [13]	For single look & Multi-look POLSAR data		Target-to-clutter ratio=6db, probability of false alarm rate = $10^{-5}$	Speckle suppression in clutter region, target detection application, for thresholding	Speckle is not always fully suppressed in high textured region

The combination of combined time-delay FIR and 2-D IIR filters [9] and the extended polarimetric whitening filter and its application to target detection in polarimetric SAR images [13] & combination of cavity filters [3], low loss broadly-tunable cavity filter operating at UHF [4] can be designed for new applications in radar up to the frequency range of about 300 MHz. Microwave filters design is problem dependent of course so combination of filters and frequency consideration as per requirement can be designed.

## References

- [1] Slawomir Koziel and John W. Bandler, "Low-Cost Dimension Scaling and Tuning of Microwave Filters Using Response Features," IEEE, 2016.
- [2] Sanjay Mishra, Dr. Agya Mishra, "Chebyshev Filters for Microwave Frequency Applications A Literature Review," IJRDS- International Journal for Scientific Research and Development, vol. 3, Issue 04, 2015.
- [3] Santosh Kumar Uikey, Dr. Agya Mishra, "Cavity Filters for Microwave Application a Literature Review," IJRDS- International Journal for scientific research and development, vol. 3, Issue 04, 2015.

- [4] D. Scarbrough, D. Psychogiou, D. Peroulii, and C. Goldsmith, "Low-Loss, Broadly-Tunable Cavity Filter Operating at UHF Frequencies," IEEE, 2015.
- [5] Yashika Saini, Mithilesh Kumar, "Performance Analysis of 9th Order Chebyshev Filter at Microwave Frequencies," IEEE International Conference on Advances in Engineering & Technology Research (ICAETR-2014), August 01-02, 2014.

- [6] Mehmet Yuceer, Member, IEEE, “A Reconfigurable Microwave Compline Filter,” IEEE transactions on circuits and systems-ii: express briefs, vol. 63, no. 1, pp. 84-88, January 2016.
- [7] Amel Baha Houda ADAMOU-MITICHE, Lahcène MITICHE, “An efficient approximant for 2D digital models: Application to the 2D IIR filters synthesis,” IEEE Jordan Conference on Applied Electrical Engineering and Computing Technologies (AEECT) , 2013.
- [8] Bogdan Dumitrescu and Riitta Niemisto, “An Iterative reweighted least-squares algorithm for the design of 2D IIR filters,” IEEE Conference Publications, 12<sup>th</sup> European Signal Processing Conference, pp. 133-136, 2004.
- [9] Arjuna Madanayake, Sewwandi Wijayarathna, Chamith Wijenayak, “Combined Time-Delay FIR and 2-D IIR Filters for EARS, Radar, and Imaging Applications,” IEEE, 2014.
- [10] Pradeep kumar, “Design of Simpson Integrator at Microwave Frequency,” IEEE conference publication, 2015.
- [11] S. Wijayarathna, A. Madanayake and S. I. Hariharan and L.T. Bruton Electrical and Computer Engineering, “Reconfigurable Phase-Linearizer for 2-D IIR RF-to-Bits Antenna-Array Digital Beam filters,” IEEE , 2013.
- [12] M. Moallem and K. Sarabandi, “A Spatial Image rejection filter based on miniaturized-element FSS for J-band radar applications,” IEEE, 2012.
- [13] Wei Gao, Fan Yang, Yi Cui, Member, IEEE, and Jian Yang, Senior Member, “The Extended Polarimetric Whitening Filter and Its Application to Target Detection in Polarimetric Synthetic Aperture Radar Images,” IEEE geoscience and Remote Sensing Letters, vol. 13, No. 3, pp. 419-423, March 2016.